Biomaterials 30 (2009) 3183–3188

Contents lists available at ScienceDirect

Biomaterials

journal homepage: www.elsevier.com/locate/biomaterials

Nanoporous gold film encapsulating cytochrome *c* for the fabrication of a H_2O_2 biosensor

Anwei Zhu, Yang Tian*, Haiqing Liu, Yongping Luo

Department of Chemistry, Tongji University, 1239 Siping Road, Shanghai 200092, People's Republic of China

ARTICLE INFO

Article history:
Received 18 December 2008
Accepted 9 February 2009
Available online 5 March 2009

Keywords:
Nanoporous Au film
Direct electron transfer
Biosensor
Cytochrome *c*
Hydrogen peroxide (H_2O_2)

ABSTRACT

A layer-by-layer route to prepare nanoporous Au film materials on transparent ITO substrates is reported by alternatively assembling Au and Ag nanoparticles through 1,5-pentanedithiol as a cross-linker, followed by that Ag nanoparticles are dissolved at room temperature in $HAuCl_4$ solution. Electron transfer of cytochrome *c* (cyt. *c*) – an excellent model for investigation of biomolecules, is greatly facilitated at the nanoporous Au film with electron transfer rate constant (k_s) of 3.9 s^{-1}. Meanwhile, cyt. *c* adsorped onto the nanoporous Au film still maintain its enzymatic activity toward H_2O_2. On the basis of these experimental results, the cyt. *c*-nanoporous Au film is exploited to an amperometric biosensor for H_2O_2 with high selectivity, broad linear range, low detection limit, and long stability.

1. Introduction

Porous Au has attracted significant attention recently for various applications including catalysis, fuel cells [1,2], cell imaging [3], energy storage [4], investigation of the critical behavior of liquid helium [5] and development of chemical sensors [6] due to its high surface-to-volume ratio, stability, and biocompatibility. The preparation of porous Au has been reported by the formation of a gold/silver alloy used as a precursor, followed by dealloying with concentrated nitric acid during which silver is removed [7]. Other methods, such as thermal decomposition of Au_2O_3, sublimation of iodine from Au–I_2 pressed powders [8], and dissolution of gold chloride in a dextran solution followed by heating to 600–800 °C [9] have been developed. Porous Au has also been prepared by means of electrochemical deposition from the homogeneous hexagonal mesophase of nonionic surfactants with metal salts [10]. The layer-by-layer (LbL) assembly technique has the advantage of providing a simple and versatile way to assemble metallic colloids into ultrathin films in which the film structure, thickness, and composition can be well tailored. If a multilayer film of colloidal Au alternately assembled with a pore-forming species is prepared, a gold film with interconnected and controlled pores could be prepared after the removal of the pore-forming species from the film. Taking advantage of this concept, we prepared nanoporous Au film on the transparent ITO by selective dissolution of sacrificial templates of silver particles in colloidal Au/Ag multilayer.

One of the most attractive avenues for the application of porous material is its use as a solid support for the immobilization of biomolecules such as proteins and enzymes. The successful immobilization of biomolecules onto solid substrates is a crucial, fundamental event for many aspects of bioanalytical chemistry, including biosensor engineering [11], biological electron transfer modeling systems [12] and the development of biocompatible materials [13]. Significant research efforts have focused on understanding and controlling protein adsorption at man-made substrates either as a precursor to a biosensor design or as a means of exploring fundamental properties of biological systems. A prominent example of this type of research is the direct or unmediated electrochemistry of redox-active proteins at modified electrodes [14–16]. Cyt. *c* is an excellent model for studying the electron transfer of typical metalloproteins from a structure point of view. Up to now, a number of methods have been developed to realize the direct electron transfer of cyt. *c* and subsequently to construct the H_2O_2 biosensor. Au nanoparticles (AuNPs), due to its prominent properties such as large surface-to-volume ratio, good biocompatibility, high catalytic efficiency, and strong adsorption ability, have been showing great applications in the construction of modified electrodes for protein immobilization. Several modified electrodes prepared with AuNPs have been fabricated to encapsulate proteins which have also displayed good direct electron transfer and catalytic activity [17–20].

* Corresponding author. Tel.: +86 21 65987075; fax: +86 21 65982287.
E-mail address: yangtian@mail.tongji.edu.cn (Y. Tian).

0142-9612/$ – see front matter © 2009 Elsevier Ltd. All rights reserved.
doi:10.1016/j.biomaterials.2009.02.019

In this work, AuNPs were firstly employed, together with LBL and SAM techniques, to construct a nanoporous Au film on transparent ITO surface using colloidal silver as a pore-forming species in the colloidal Au/Ag multilayer films, for the immobilization of cyt. *c*. The purely porous Au nanostructures were fabricated in a mild and template-independent way, together with the potential ability to provide a uniform surface environment for the adsorption of biomolecules across a large surface area.

2. Experimental

2.1. Materials

Hydrogen tetrachloroaurate ($HAuCl_4 \cdot 3H_2O$), 1,5-pentanedithiol (noted as dithiol), poly(diallyldimethylammonium chloride) (PDDA, aqueous solution with a molecular weight of 100,000–200,000), horse heart cytochrome *c* (cyt. *c*, MW 12,384) were purchased from Sigma–Aldrich. All other reagents were of analytical grade, and double distilled water was used throughout. ITO-coated glass plates with a square resistance of $\sim 10\,\Omega\,cm^{-2}$ were purchased from Shenzhen Nanbo Display Technology Co. Ltd. (Shenzhen, China).

2.2. Preparation and modification of nanoporous Au film

The Au colloids were prepared by the conventional $NaBH_4$ reduction of $HAuCl_4$ in water [21]. The colloidal Ag nanoparticles were prepared in a similar way to that of colloidal Au except $HAuCl_4$ was replaced with $AgNO_3$. Transmission electron microscopy (TEM) revealed an average diameter of 5 ± 1.2 nm and 10 ± 2.4 nm for colloidal Au and Ag respectively (Supplementary Information, Fig. S1). ITO-coated glass plate was used as substrate and was cleaned by sonicating sequentially for about 30 min each in acetone, 10% KOH in ethanol, and distilled water.

As schematically shown in Fig. 1, the prepared ITO electrode with original negative surface charge was first treated with an aqueous solution of PDDA (1 mg/mL) for about 30 min to form positively charged surface. After the treated substrate was washed with distilled water and dried, it was immersed in colloidal Au solution for 5 min followed by extensively rinsing with water and drying with nitrogen gas. This substrate was then immersed in a 10 mM alcoholic solution of 1,5-pentanedithiol for 5 min followed by rinsing with abundant ethanol and drying with nitrogen gas. The 1,5-pentanedithiol-covered substrate was then adsorped in Ag colloids for 5 min followed by extensively rinsing with water and drying with nitrogen gas to obtain a layer of Ag colloids. By repeating the above steps in a cyclic fashion, composite multilayer films $(Au/Ag)^*n$ with *n* referring to the number of deposition cycles was fabricated. After complete dissolution of Ag nanoparticles by immersing the multilayer films in a mixture of an aqueous solution of 3.0 mM $HAuCl_4$ and 3 M NaCl, a nanoporous Au film was obtained. The as-prepared nanoporous Au film was adsorped in 25 mM PBS (pH 7.2) containing 0.2 mM cyt. *c* for about 30 min at 4 °C in refrigerator. Hereafter, cyt. *c* modified nanoporous Au electrode will be referred as cyt. *c*/porous Au/ITO.

2.3. Instrumentations and measurements

Cyclic voltammetric (CV) and amperometric measurements were carried out by a computer-controlled CHI 660C electrochemical workstation (Shanghai, China) in a home-made three-electrode electrochemical cell using a KCl-saturated Ag/AgCl electrode as reference electrode and a platinum wire as auxiliary electrode. The supporting electrolyte was 25 mM phosphate buffer solution (PBS, pH 7.2), which was prepared with KH_2PO_4 and K_2HPO_4. The PBS was purged with high-purity nitrogen for at least 30 min prior to experiments and a nitrogen atmosphere was kept over the solution in the cell. In steady-state amperometric experiment, the potential was set as at −0.1 V with a stirring rate of 200 rpm, and the current–time curves were recorded after a constant background current had been established. All electrochemical experiments were performed at the room temperature. UV–vis absorption spectrum was recorded by an Agilent 8453 UV–vis–NIR spectrophotometer (Agilent instruments). SEM images were taken by a Quanta 200 FEG (FEI Company). TEM images were taken by a JEM-1230 (JEOL Company).

3. Results and discussion

3.1. Characterization of nanoporous Au films

To prepare nanoporous Au films, a precursor film in which Ag nanoparticles are well dispersed in layers of Au nanoparticles are required. For this aim, multilayer films comprised of nonsaturated layers of colloidal Au and Ag were employed. UV–vis spectra of colloidal Au and Ag in solution show a plasmon absorption peak at 519 and 395 nm, respectively (Supplementary Information, Fig. S2). These plasmon absorption peaks remain in the solid films with a slight red-shift compared with those in solution and therefore can be used to monitor the adsorption dynamics of colloidal Au and Ag. Colloidal Au or Ag was adsorbed at different time intervals on a 1,5-pentanedithiol-modified ITO slide, and its absorbance at λ_{max} was recorded. The absorbance both increased drastically in the beginning and gradually reached constant after 20 min of adsorption. Herein, a 5 min immersion time in colloidal Au and Ag solutions was used to construct Au/Ag multilayer.

The construction process of the composite Au/Ag multilayer on ITO slides was monitored by UV–vis spectroscopy. As shown in Fig. 2, the first adsorbed layer (line 1) of Au nanoparticles has a plasmon absorption peak at 531 nm, which is 12 nm red-shifted compared with that in solution due to the change of refractive index. When a second layer (line 2) of Ag nanoparticles was adsorbed, the typical plasmon absorption peak of nonaggregated colloidal Ag at 400 nm appeared with the absorbance between 200 and 700 nm all increasing at the same time. The absorbance

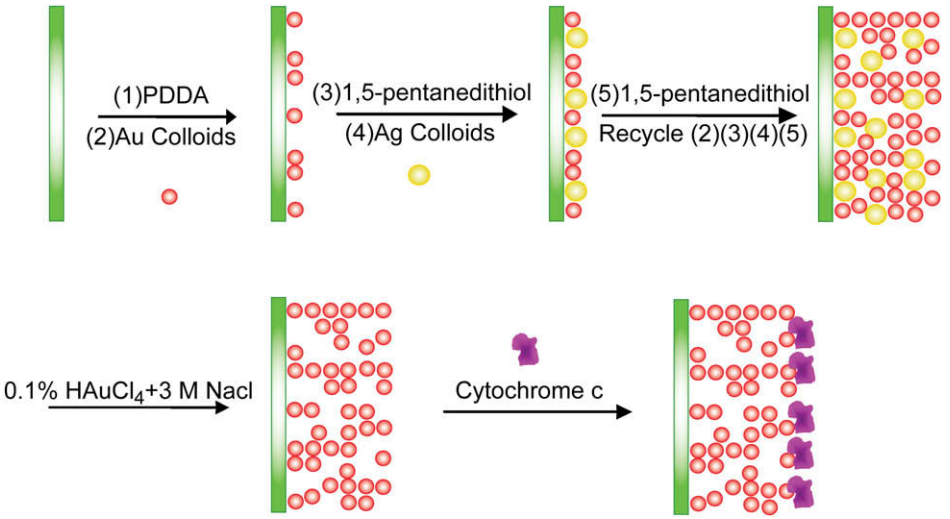

Fig. 1. Schematic illustration of preparing process of cyt. *c*/nanoporous Au/ITO electrode.

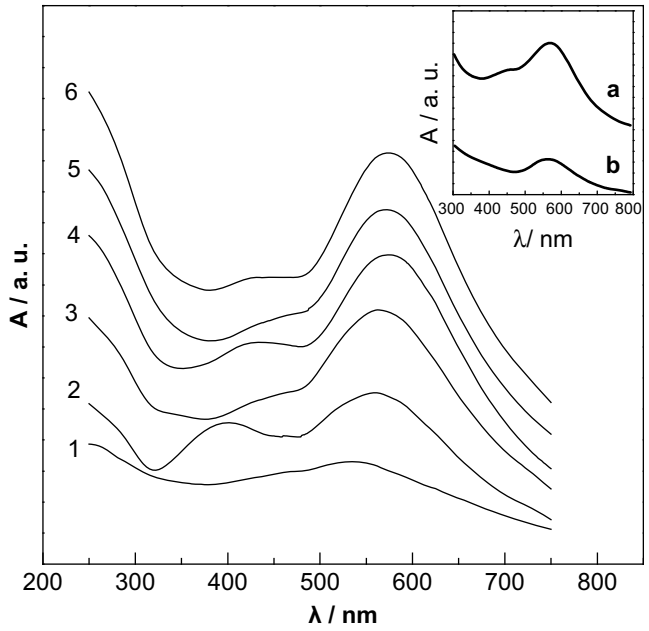

Fig. 2. UV–vis absorption spectra of multilayer of colloidal Au/Ag with different numbers of layers deposited on an ITO slide. Inset: absorption spectra of a $(Au/Ag)^*3/Au$ multilayer film after immersion in a mixture solution of 3.0 mM $HAuCl_4$ and 3 M NaCl for (a) 0, (b) 60 s.

increased with the adsorption of colloidal Au and Ag (lines 1–6), confirming the successful construction of Au/Ag multilayer.

As shown in Fig. 1, nanoporous Au films were prepared by selective dissolution of sacrificial templates of Ag nanoparticles. Because the standard reduction potential of the $AuCl_4^-/Au$ pair (0.99 V, versus SHE) is higher than that of the Ag^+/Ag pair (0.80 V, versus SHE), silver nanoparticles loaded in solid films can be oxidized by $HAuCl_4$ according to the following replacement reaction: $AuCl_{4(aq)}^- + 3Ag_{(s)} \rightarrow Au_{(s)} + 3Ag^+_{(aq)} + 4Cl^-_{(aq)}$. But precipitates of AgCl produced during the oxidation process passivate

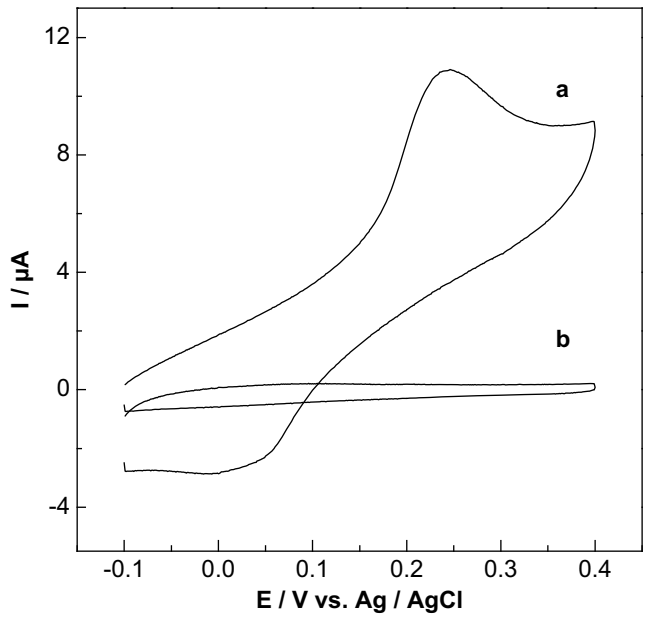

Fig. 3. Cyclic voltammograms of an ITO electrode deposited with $(Au/Ag)^*3/Au$ multilayer after immersion in a mixture solution of 3.0 mM $HAuCl_4$ and 3 M NaCl for (a) 0 s, (b) 60 s. The solution is 0.1 M phosphate buffer (pH 7.0), and the scan rate is 10 mV/s. An Ag/AgCl electrode was used as a reference electrode.

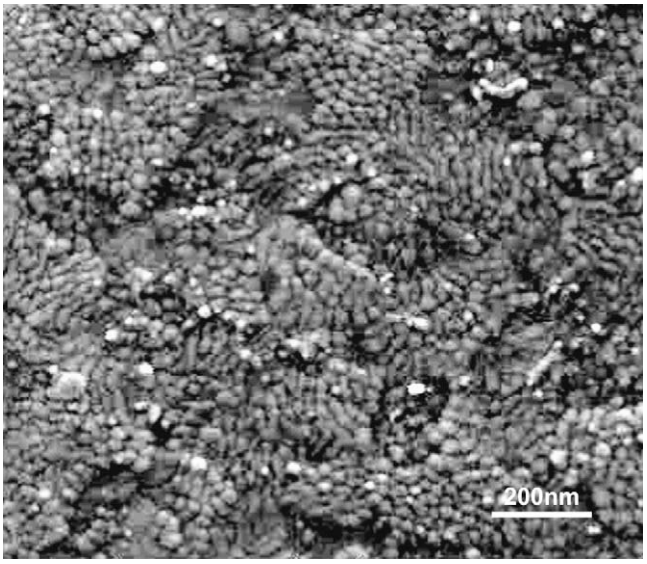

Fig. 4. SEM image of nanoporous Au modified ITO electrode.

colloidal Ag, leading to cease of the oxidation reaction. When the concentration of Cl^- ions reach 2.8 M, complexes of Ag^+ and Cl^- ($AgCl_n^{(n-1)-}$) are formed which are soluble in water (96% of silver ions are in the form of $AgCl_4^{3-}$ according to literature) [22]. Therefore, a mixture solution of 3.0 mM $HAuCl_4$ and 3 M NaCl was used to dissolve the colloidal Ag in the composite Au/Ag multilayer, just as follows: $AuCl_{4(aq)}^- + 3Ag_{(s)} + (3n-4)Cl^-_{(aq)} \rightarrow Au_{(s)} + 3AgCl_n^{(n-1)-}{}_{(aq)}$. As illustrated in the inset of Fig. 2, UV–vis spectroscopy shows that the complete dissolution of Ag nanoparticles takes place in the mixture solution after 1 min. Because of the overlap of surface plasmon absorption peak of colloidal Ag and Au in the visible region, the dissolution process of colloidal Ag was further confirmed by the CVs of colloidal Ag/Ag multilayer before and after removal of colloidal Ag in 0.1 M PBS with a scan rate of 10 mV/s. As shown in Fig. 3, in the potential scan ranging from −0.1 to 0.4 V, only one pair of redox peaks, which correspond to the reduction/oxidation of colloidal Ag, are observed for the multilayer [23]. After the electrode was immersed in the mixture solution for 60 s, the redox peaks disappeared completely, indicating the complete removal of Ag nanoparticles deposited in the film. This result agrees well with that obtained by UV–vis spectroscopy. The structure of the nanoporous Au film was also examined with FE–SEM (see Fig. 4). It clearly demonstrates a highly porous film, with a ligament size of 13.4 ± 4.6 nm, which is a little larger than that of the prepared Ag particle, possibly due to some aggregates of Ag nanoparticles or colloidal Au/Ag.

3.2. Bioactivity of cyt. c immobilized on nanoporous Au films

The position of the Soret absorption band of iron heme provides information about conformation of heme proteins [24]. The peak will be diminished if the protein is denatured [25]. Fig. 5 depicts UV–vis absorption spectra of 0.2 mM cyt. *c* in solution (a) and cyt. *c* confined on the nanoporous Au surface (b). The band for cyt. *c* adsorbed on the nanoporous Au film is located at 411 nm, just a 2-nm red-shift compared with that of native cyt. *c* solution (409 nm). A shift of only 2 nm suggests that the microenvironment of the proteins was slightly changed but no significant denaturation occurred. This also implies that the nanoporous Au matrix has good biocompatibility and is suitable for cyt. *c* molecules to maintain their native conformation and bioactivity.

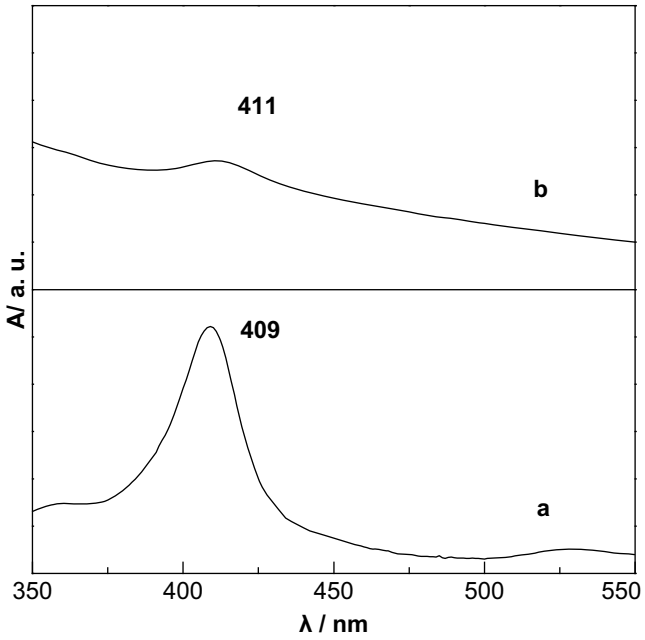

Fig. 5. UV–vis absorption spectra of (a) 0.2 mM cyt. *c* solution and (b) cyt. *c* adsorbed on the nanoporous Au film.

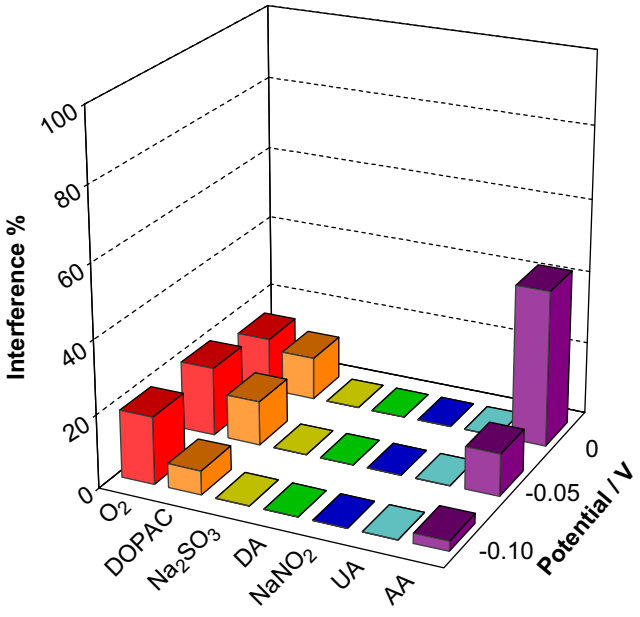

Fig. 7. The selectivity profile obtained at different applied potentials: −0.10, −0.05, 0 V versus Ag/AgCl.

3.3. Direct electrochemistry of cyt. c at nanoporous Au film

Fig. 6 shows typical cyclic voltammograms of the nanoporous Au film (a) and cyt. *c*/porous Au/ITO electrode (b) in 25 mM PBS (pH 7.2). While only charge current was observed at the nanoporous Au surface (a), a pair of redox peaks of cyt. *c* with a peak width at half peak height ($\Delta E_{p,1/2}$) of 65 mV was observed at the cyt. *c* modified nanoporous Au film (b). The formal potential ($E^{0'} = (E_{p,a} + E_{p,c})/2$) of cyt. *c* confined on the nanoporous Au film is estimated to be 9.3 mV versus Ag/AgCl. A linearity of the cathodic or anodic peak currents with scan rates (inset in Fig. 6) indicates that the redox process is confined to the surface [26]. In addition, the CVs remained essentially unchanged on consecutive potential scanning up to 1000 cycles at sweep rate of 50 mV/s, confirming that the immobilized cyt. *c* was stable. The kinetics of the heterogeneous electron transfer can be analyzed by the model of Laviron [27]. The electron transfer rate constant, k_s, was estimated to be 3.9 s^{-1} according to the formula $m = (RT/F)(k_s/nv)$, where m is a parameter related to the peak-to-peak separation [28]. It is much higher than that of cyt. *c* adsorbed on ordered mesoporous niobium oxide film (0.28 s^{-1}) [18], NaY zeolite/GCE ($0.78 \pm 0.04\ s^{-1}$) [29], slightly higher than that of colloidal Au/carbon paste ($1.21 \pm 0.08\ s^{-1}$) [28],

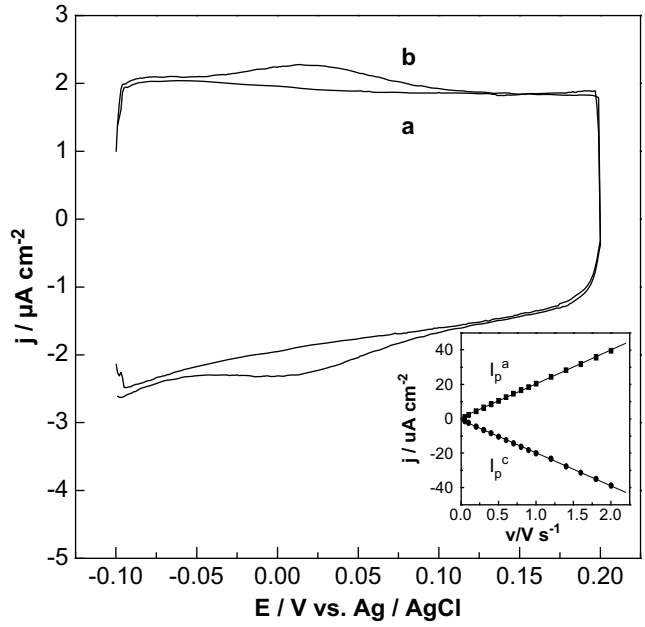

Fig. 6. CVs obtained at (a) nanoporous Au film and (b) cyt. *c*/nanoporous Au film in 25 mM PBS (pH7.2); Potential scan rate: 100 mV/s. Inset: relationship between cathodic and anodic currents of the cyt. *c*/nanoporous Au electrode and scan rate.

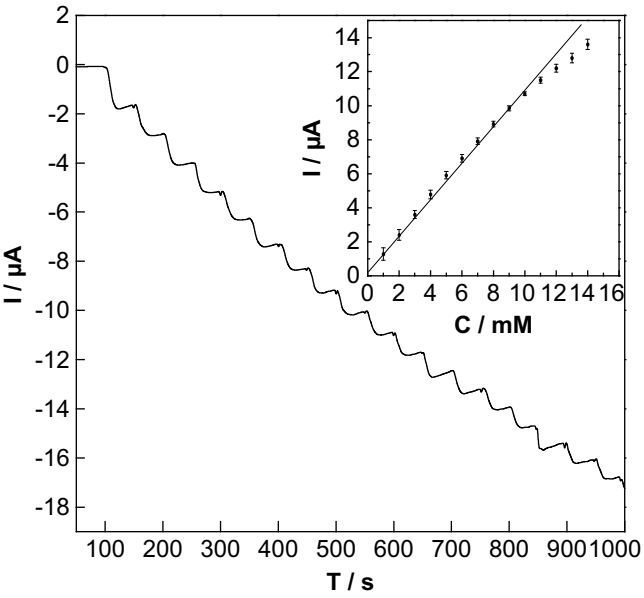

Fig. 8. Typical amperometric responses of the cyt. *c* modified nanoporous gold film to successive addition of 1×10^{-3} M H_2O_2 at −0.1 V in 25 mM PBS (pH = 7.2). Inset: calibration plot of steady-state currents against concentrations of H_2O_2.

Table 1
Comparison of the performance of different hydrogen peroxide sensors based on AuNPs.

Nanocomposites	Applied potential (mV)	Detection limit (M)	Linear range (M)	Response time (s)	Reference
Cyt. *c*/Nanoporous Au	−100[a]	6.3×10^{-6}	1×10^{-5}–1.2×10^{-2}	8	[c]
Cyt. *c*/Au-NR	−100[a]	3.7×10^{-6}	5×10^{-5}–1.5×10^{-3}	5	[20]
Cyt. *c*/Au/CP	−100[a]	1×10^{-5}	1×10^{-5}–1×10^{-3}	–	[28]
Cyt. *c*/Au/Chit	−250[b]	9.8×10^{-6}	8.5×10^{-4}–1.3×10^{-2}	8	[32]
HRP/Clay/Chit/Au	−300[a]	9×10^{-6}	3.9×10^{-5}–3.1×10^{-3}	–	[33]
HRP/Au/TiO_2	−600[a]	2×10^{-6}	5×10^{-6}–4×10^{-4}	5	[34]

Au-NR, nanorod-like Au; CP, carbon paste; Chit, Chitosan; HRP, Horseradish peroxidase.
[a] Versus Ag/AgCl.
[b] Versus SCE.
[c] The present work.

L-cysteine/Au ($1.25 \pm 0.10\ s^{-1}$) [30], and SiO_2/cyt. *c*/SiO_2/boron-doped diamond ($1.39\ s^{-1}$) [31]. This faster electron transfer rate indicates that nanoporous Au film provided an excellent biocompatible surface for the electron transfer of cyt. *c*. By integration of the anodic peaks in CV, the charges and thus the average surface concentration of electroactive species could be calculated. The average surface concentration of electroactive cyt. *c* adsorbed on the nanoporous Au film was estimated to be 2.81×10^{-12} mol cm^{-2}. Taking account of the size ($2.6 \times 3.2 \times 3.0$ nm) of cyt. *c* molecule, cyt. *c* molecules might be adsorbed on the nanoporous Au film in a monolayer.

3.4. An amperometric biosensor for H_2O_2

The direct electron transfer of cyt. *c* was enhanced at the nanoporous Au film, and cyt. *c* immobilized on the nanoporous Au almost processed the enzymatic activity toward H_2O_2. These results provided us a strong basis to construct an amperometric biosensor for H_2O_2 because the heme has been well documented as the active site for the catalysis to the reduction of H_2O_2.

There is no doubt that the sensitivity of electrochemical biosensors is strongly dependent on the applied potential. The cathodic current of H_2O_2 obtained at cyt. *c*/nanoporous Au film increased with the negative shift of the operating potentials (data not shown). This observation gives the experimental basis for choosing the suitable operating potential for the measurement of H_2O_2. On the other hand, the selectivity of electrochemical biosensors is also potential-dependent. To the best of our knowledge, the coexisting biological compounds, such as AA, O_2, and so on may interfere with the electrochemical determination of H_2O_2. Fig. 7 demonstrates eight kinds of potential interferences under different applied potentials. At the more positive potentials, e.g., −0.05 and 0 V, 11.5 and 42.8% anodic currents of 0.1 mM AA were obtained relative to 0.1 mM H_2O_2. Meanwhile, as the potential was more negatively shifted, the interference from O_2 became slightly higher. Therefore, to fulfill both selectivity and sensitivity of the present biosensor, −0.1 V (versus Ag/AgCl) was selected as the optimized operating potential.

Fig. 8 shows a typical current–time plot of the cyt. *c*/nanoporous Au/ITO electrode on successive addition of 1 mM H_2O_2 into stirring PBS (25 mM, pH 7.2) at the applied potential of −0.1 V. The calibration plot is depicted in the inset of Fig. 8. Well-defined steady-state current responses were obtained in 8 s at this applied potential, and the currents increased stepwise with successive additions of H_2O_2. The sensitivity of the present H_2O_2 biosensor is 2.8 ± 0.2 mA cm^{-2} M^{-1}. The analytical characteristic of the present H_2O_2 biosensor at the optimum conditions is summarized in Table 1. For comparison, other previously attained H_2O_2 biosensors based on direct electron transfer of proteins at nanostructured Au are also listed in Table 1. In contrast with other H_2O_2 biosensors reported so far, besides higher selectivity, cyt. *c*/porous Au/ITO electrode shows excellent analytical performance, for instance, wider linear detection range and short response time.

For the stability test, response current for H_2O_2 was recorded 2 times daily and the current responses were found to be constant for at least 1 month, which holds relatively longer stability than that obtained at other H_2O_2 biosensors. In addition, we have found that the deviation of the current responses of over 5 sensors prepared with the same method did not exceed 7.2% (RSD).

4. Conclusions

Nanoporous Au film was successfully fabricated through a low-cost and template-independent way and the prepared nanostructures were achieved for the direct electron transfer of cyt. *c*. The enhanced electron transfer of cyt. *c* adsorbed on the porous Au film associated with the inherent catalytic activity of heme toward H_2O_2, provided us to develop an amperometric H_2O_2 biosensor. The analytical characteristics, together with the intrinsic properties of Au nanoparticles sufficiently gave a strong basis for continuous detection of H_2O_2 under pathophysiological conditions. The present investigation not only provided a methodology to prepare nanoporous metal film with tunable size, but also opened a way to realize direct electron transfer of enzymes, and based on this platform to construct other biosensors.

Acknowledgements

This work was financially supported by the Program for New Century Excellent Talents in University (NCET-06-0380) and the Scientific Research Foundation for the Returned Overseas Chinese Scholars, from State Education Ministry, China, and Shanghai Pujiang Program (06PJ14090). Tongji University is also greatly acknowledged.

Appendix. Supplementary information

Supplementary data associated with this article can be found in the online version at doi:10.1016/j.biomaterials.2009.02.019.

References

[1] West JL, Hatas NJ. Engineered nanomaterials for biophotonics applications: improving sensing, imaging, and therapeutics. Annu Rev Biomed Eng 2003;5:285–96.
[2] Ding Y, Chen M, Erlebacher J. Metallic mesoporous nanocomposites for electrocatalysis. J Am Chem Soc 2004;126:6876–7.
[3] Shukla S, Priscilla A, Banerjee M, Bhonde R, Ghatak J, Satyam PV, et al. Porous gold nanospheres by controlled transmetalation reaction: a novel material for application in cell imaging. Chem Mater 2005;17:5000–5.
[4] Gregory S, Torsten R, Burkhard R. Energy storage by the electrochemical reduction of CO_2 to CO at a porous Au film. J Electroanal Chem 2002;526:125–33.
[5] Csathy GA, Tulimieri D, Yoon J, Chan MHW. Heat capacity and superfluid density of thin He films on porous gold and on H_2. Phys Rev Lett 1998;80:4482–5.
[6] Bonroy K, Friedt J-M, Frederix F, Laureyn W, Langerock S, Campitelli A, et al. Realization and characterization of porous gold for increased protein coverage on acoustic sensors. Anal Chem 2004;76:4299–306.
[7] Erlebacher J, Aziz M, Karma A, Dimitrov N, Sieradzki K. Evolution of nanoporosity in dealloying. Nature 2001;410:450–3.
[8] Jurczakowski R, Hitz C, Lasia A. Impedance of porous Au based electrodes. J Electroanal Chem 2004;572:355–66.

[9] Walsh D, Arcelli L, Ikoma T, Tanaka J, Mann S. Dextran templating for the synthesis of metallic and metal oxide sponges. Nat Mater 2003;2:386–90.
[10] Attard GS, Bartlett PN, Coleman NRB, Elliott JM, Owen JR, Wang JH. Mesoporous platinum films from lyotropic liquid crystalline phases. Science 1997;278:838–40.
[11] Nam JM, Shad TC, Mirkin CA. Nanoparticle-based bio-bar codes for the ultrasensitive detection of proteins. Science 2003;301:1884–6.
[12] Bowden EF. Wiring mother nature. Interfacial electrochemistry of proteins. Electrochem Soc Interface 1997;6:40–4.
[13] Schoenfisch MH, Mowery KA, Rader MV, Baliga N, Wahr JA, Meyerhoff ME. Improving the thromboresistivity of chemical sensors via nitric oxide release: fabrication and in vivo evaluation of NO-releasing oxygen-sensing catheters. Anal Chem 2000;72:11119–26.
[14] Leger C, Bertrand P. Direct electrochemistry of redox enzymes as a tool for mechanistic studies. Chem Rev 2008;108:2379–438.
[15] Zugates GT, Anderson DG, Little SR, Lawhorn IEB, Langer R. Synthesis of poly(b-amino ester)s with thiol-reactive side chains for DNA delivery. J Am Chem Soc 2006;128:12726–34.
[16] Kontos HA, Wei EP. Superoxide production in experimental brain injury. J Neurosurg 1986;64:803–7.
[17] Qiu HJ, Xu CX, Huang XR, Ding Y, Qu YB, Gao PJ. Adsorption of laccase on the surface of nanoporous gold and the direct electron transfer between them. J Phys Chem C 2008;112:12781–5.
[18] Zhao J, Zhu XL, Li T, Li GX. Self-assembled multilayer of gold nanoparticles for amplified electrochemical detection of cytochrome *c*. Analyst 2008;133:1242–5.
[19] Shulga OV, Jefferson K, Khan AR, D'Souza VT, Liu JY, Demchenko AV, et al. Preparation and characterization of porous gold and its application as a platform for immobilization of acetylcholine esterase. Chem Mater 2007;19:3902–11.
[20] Liu HQ, Tian Y, Xia PP. Pyramidal, rodlike, spherical gold nanostructures for direct electron transfer of copper, zinc–superoxide dismutase: application to superoxide anion biosensors. Langmuir 2008;24:6359–66.
[21] Brown KR, Walter DG, Natan MJ. Seeding of colloidal Au nanoparticle solutions. 2. Improved control of particle size and shape. Chem Mater 2000;12:306–13.
[22] Lampre I, Pernot P, Mostafavi M. Spectral properties and redox potentials of silver atoms complexed by chloride ions in aqueous solution. J Phys Chem B 2000;104:6233–9.
[23] Nair AS, Tom RT, Suryanarayanan V, Pradeep T. ZrO_2 bubbles from core–shell nanoparticles. J Mater Chem 2003;13:297–300.
[24] George P, Hanania G. A spectrophotometric study of ionizations in methaemoglobin. J Biochem 1953;55:236–43.
[25] Nassar AF, Willis WS, Rusling JF. Electron transfer from electrodes to myoglobin: facilitated in surfactant films and blocked by adsorbed biomacromolecules. Anal Chem 1995;67:2386–92.
[26] Bard AJ, Faulkner LR. Electrochemical methods. Fundamentals and applications. 2nd ed. New York: Wiley; 2001.
[27] Laviron E. General expression of the linear potential sweep voltammogram in the case of diffusionless electrochemical systems. J Electroanal Chem 1979;101:19.
[28] Ju HX, Liu SQ, Ge BX, Lisdat F, Scheller FW. Electrochemistry of cytochrome *c* immobilized on colloidal gold modified carbon paste electrodes and its electrocatalytic activity. Electroanalysis 2002;14:141–7.
[29] Dai ZH, Liu SQ, Ju HX. Direct electron transfer of cytochrome *c* immobilized on a NaY zeolite matrix and its application in biosensing. Electrochemica Acta 2004;49:2139–44.
[30] Liu YC, Cui SQ, Zhao J, Yang ZS. Direct electrochemistry behavior of cytochrome *c*/L-cysteine modified electrode and its electrocatalytic oxidation to nitric oxide. Bioelectrochemistry 2007;70:416–20.
[31] Geng R, Zhao GH, Liu MC, Li MF. A sandwich structured SiO_2/cytochrome *c*/SiO_2 on a boron-doped diamond film electrode as an electrochemical nitrite biosensor. Biomaterials 2008;29:2794–801.
[32] Feng JJ, Zhao G, Xu JJ, Chen HY. Direct electrochemistry and electrocatalysis of heme proteins immobilized on gold nanoparticles stabilized by chitosan. Anal Biochem 2005;342:280–6.
[33] Zhao XJ, Mai ZB, Kang XH, Zou XY. Direct electrochemistry and electrocatalysis of horseradish peroxidase based on clay-chitosan-gold nanoparticle nanocomposite. Biosens Bioelectron 2008;23:1032–8.
[34] Kafi AKM, Wu GS, Chen AC. A novel hydrogen peroxide biosensor based on the immobilization of horseradish peroxidase onto Au-modified titanium dioxide nanotube arrays. Biosens Bioelectron 2008;24:566–71.